High-Performance Solar MPPT Using Switching Ripple Identification Based on a Lock-In Amplifier

Francisco Paz, *Student Member, IEEE*, and Martin Ordonez, *Member, IEEE*

Abstract*—Photovoltaic (PV) power converters and maximum power point tracking (MPPT) algorithms are required to ensure maximum energy transfer between the PV panel and the load. The requirements for the MPPT algorithms have increased over the years—the algorithms are required to be increasingly accurate, fast, and versatile, while reducing the intrusiveness on the overall performance of the PV panel and converter. The family of hill-climbing algorithms such as incremental conductance (InCond) and perturb and observe (P&O) has gained popularity given their simplicity and accuracy, but it requires the injection of a perturbation that changes the operating point even in steady state and are prone to errors during changing environmental conditions. In recent literature, the use of the switching ripple has been proposed to replace the perturbation in the hill-climbing algorithms given its inherent presence in the system and speed. The constant work toward smaller and faster ripples presents challenges to the signal detection involved in this kind of algorithm. This paper develops and implements a new InCond MPPT technique based on switching ripple detection using a digital lock-in amplifier (LIA) to extract the amplitude of the oscillation ripple even in the presence of noise. The use of this advanced technique allows to push forward the reduction of the ripple in order to virtually eliminate the oscillation in steady state maximizing the efficiency. The accurate detection allows for adaptive-step features for fast tracking of changing environmental conditions while keeping the efficiency at maximum during the steady state. Detailed mathematical analysis of the proposed technique is provided. Overall, the use of the proposed LIA allows to push the reduction of the ripple even more while keeping accuracy and delivering superior performance. Simulations and experimental results are provided for the proposed technique and the InCond technique in order to validate the proposed approach.

***Index Terms*—Incremental conductance (InCond), lock-in amplifier, maximum power point tracking (MPPT), solar power generation.**

Manuscript received August 20, 2015; revised November 25, 2015; accepted January 1, 2016. Date of publication February 16, 2016; date of current version May 10, 2016. This work was supported by the Natural Sciences and Engineering Research Council of Canada (NSERC).

The authors are with the Department of Electrical and Computer Engineering, The University of British Columbia, Vancouver, BC V6T 1Z4, Canada (e-mail: franciscopaz@ieee.org; mordonez@ieee.org).

Color versions of one or more of the figures in this paper are available online at http://ieeexplore.ieee.org.

Digital Object Identifier 10.1109/TIE.2016.2530785

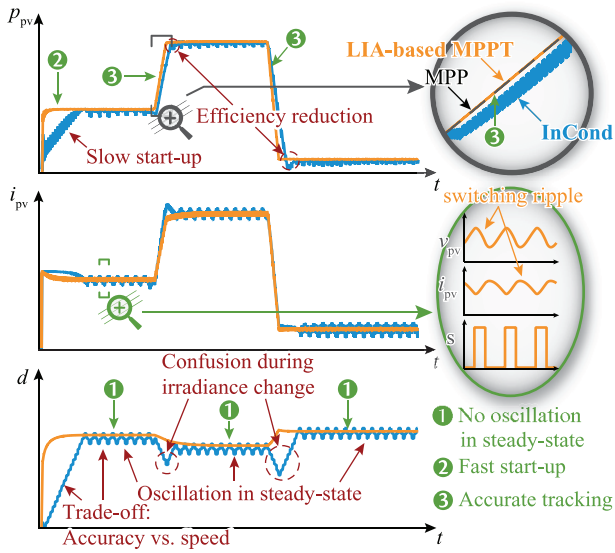

Fig. 1. Comparison between the proposed MPPT algorithm (orange trace) and the standard InCond algorithm (blue trace). The issues of the InCond show oscillations in steady-state slow start-up, confusion during irradiance changes, and a trade-off between speed and accuracy. The proposed LIA-based MPPT algorithm uses the switching ripple in the power converter to accurately track the MPP with no perturbation, fast start-up and tracking due to the identification and the integral controller.

I. Introduction

PEAK energy harvesting for photovoltaic (PV) panels has become a fundamental requirement to achieve overall conversion performance. Ensuring the PV panel operates at the maximum power point (MPP) is entrusted to the maximum power point tracking (MPPT) algorithm. Many contributions have been implemented in the past years to tackle this problem [1], but some issues remain open. A wide variety of MPPT algorithms are available [2], [3] ranging from simple and inaccurate algorithms such as the constant voltage (CV), fractional open circuit voltage (FOCV) or fractional short circuit current (FSCI); the popular hill-climbing algorithms such as the perturb and observe (P&O) and the incremental conductance (InCond) [4]; and the complex algorithms based on heuristics such as particle swarm optimization (PSO) [5], [6] and Fuzzy logic [7], [8].

The popularity of the hill-climbing techniques (InCond and P&O) derives from their simplicity, needing few sensors and tuning parameters. They work by injecting a change in the operating point of the converter (perturbation) and checking for a

condition to determine the better operating point. However, several issues remain unsolved. Both the InCond and the P&O algorithms suffer from a characteristic oscillation in steady state that derives in a reduction of the efficiency [9], [10]. The step-size of the algorithm and the sampling-time are mixed to produce a trade-off between accuracy and speed [11]–[13] that leaves the fast algorithms with large oscillations and the accurate algorithms with slow tracking speed; this has lead to optimization criteria [14]–[16] and adaptive versions of the algorithm [17], [18]. Among the adaptive versions of the algorithm, new approaches have been presented using dual Kalman filters on field programable gate array (FPGA) devices [19], [20], this technique is used to identify parameters from the system and adapt the MPPT algorithm for optimization. Another common problem of the InCond and P&O is the tracking of changing environmental conditions, namely the irradiance and the temperature (T). The nature of the algorithm leads to confusion during changing conditions and inefficient tracking even when going in the correct direction [21], [22]. Solutions have been presented for some of the issues such as environmental changes [23] and local maxima problems [24]–[29]. An important limitation to the classical approaches is based on the measurement of the effect of the step; the switching ripple and low-frequency ripple can interact with measurement and make a confusion, solutions have been proposed to minimize this interaction while keeping the standard algorithms [30], [31]. Opportunities to introduce further improvements in steady-state operation and transient dynamic tracking remain open. Work toward reducing the size of the perturbation has been explored recently [32], [33]. It has been shown in [34] and [35] that the switching ripple can be used as a nonintrusive method to perform optimization. The elimination of perturbation and use of existing switching ripple have the potential to increase MPPT performance but switching ripple is hard to detect (very small and noisy). These features are of special significance for power converters of medium- to high-power subject to changing environmental conditions such as electric/hybrid vehicles [36]–[38].

In this paper, an algorithm will be developed to provide high-switching ripple detection and tracking abilities in the presence of noise to allow small ripple detection and high MPPT performance. A digital processing technique will be used to identify InCond from the ripple and successfully produce a single-loop MPPT-oriented control to track dynamically while eliminating any undesired perturbations. The implementation will be done with a robust LIA and will feature real-time identification and remarkable performance in steady and transient operation. The LIA has been used in the past to characterize the impedance in fuel cells [39], transformers [40], and other devices [41], but not explored in Solar MPPT applications as proposed in this work. In [33], a fixed frequency sinusoidal oscillation is injected in the system, an LIA is used to extract the amplitude of the oscillation; this has the disadvantage of needing to inject an artificial oscillation slower than the control loops, which in turn are slower than the switching frequency. The novel MPPT technique based on LIA will advantage of the existing switching ripple and provide adaptive-steps resulting in enhanced performance. The three key features that want to be achieved by this algorithm are outlined in Fig. 1 in comparison with the standard InCond algorithm: using the switching ripple to estimate the conductance allows for smooth operation in steady-state ❶, fast, and accurate start-up ❷, and accurate tracking during the transients with no errors ❸. Simulations and experimental results implemented in an industry-standard microcontroller are provided to assess the performance of the proposed strategy and a comparison is performed with existing high-performance algorithms.

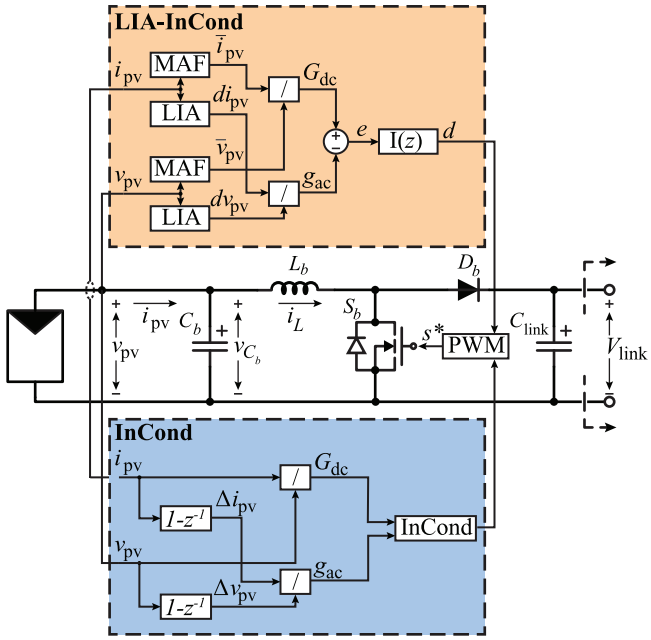

Fig. 2. Schematic of the converter and the MPPT algorithms.

II. System Model

The block diagram of the proposed system is presented in Fig. 2. It includes a PV panel supplying energy to a dc bus through a boost converter. The dc bus is assumed to be able to take all the energy available from the PV panel, therefore, making it useful to have MPPT. The i_{pv} and v_{pv} are regulated by the power converter to match the impedance of the load to that of the converter ensuring maximum power transfer. Two MPPT algorithms are implemented: the proposed LIA-based MPPT and the standard InCond in order to compare them. The standard InCond algorithm is selected as a baseline comparison because most modern MPPT algorithms are at some point compared with the InCond; by comparing with this algorithm, it is possible to extend the comparison to other existing algorithms and future improvements. As it can be observed in Fig. 2 the algorithm directly drives the duty-cycle, producing MPPT-oriented control algorithms that maximize speed while reducing complexity.

In this section, a model of the PV panel is presented, detailing the behavior and the characteristics that ensure the maximum power transfer. A summary of the basic InCond MPPT algorithm is introduced and its limitations are discussed.

A. PV Panel Background

The equivalent circuit of a PV cell is presented in Fig. 3(a). For M equal strings of N series connected cells, the characteristic curve is given by

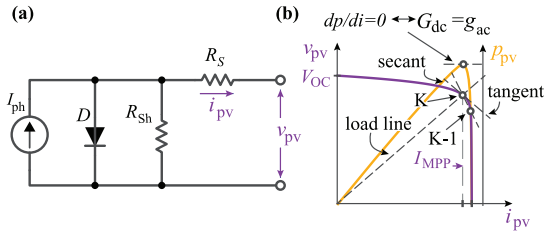

Fig. 3. (a) Equivalent circuit of a PV cell is presented. (b) $V-I$ and $P-I$ characteristics of the PV cell are presented.

$$i_{\mathrm{pv}} = MI_{\mathrm{ph}} - MI_0\left(e^{\frac{v_{\mathrm{pv}}+i_{\mathrm{pv}}R_sN/M}{NV_T}} - 1\right) - \frac{v_{\mathrm{pv}}+i_{\mathrm{pv}}R_sN/M}{NR_{\mathrm{sh}}}. \tag{1}$$

The $V-I$ curves of the panel are presented in 3(b). In order to operate the PV panel at the MPP, the maxima has to be found. In the MPP the power characteristic has a zero derivative

$$\frac{\mathrm{d}p_{\mathrm{pv}}}{\mathrm{d}v_{\mathrm{pv}}} = 0. \tag{2}$$

Expanding (2) for the $V-I$ expressions, the condition can be stated as

$$\frac{i_{\mathrm{pv}}}{v_{\mathrm{pv}}} = -\frac{\mathrm{d}i_{\mathrm{pv}}}{\mathrm{d}v_{\mathrm{pv}}} \tag{3}$$

which is the same as

$$G_{\mathrm{dc}} = g_{\mathrm{ac}}. \tag{4}$$

This condition is represented in Fig. 3(b). The load line (whose slope is given by G_{dc}) has to be perpendicular to the tangent line at that operating point. Keeping the PV panel working in this condition under changing environmental conditions is the task of the MPPT algorithm.

B. Standard InCond MPPT Algorithm

The standard InCond MPPT algorithm scans the $I-V$ curve looking for (4). The G_{dc} is estimated as

$$\hat{G}_{\mathrm{dc}}(K) = \frac{i_{\mathrm{pv}}(K)}{v_{\mathrm{pv}}(K)} \tag{5}$$

where $i_{\mathrm{pv}}(K)$ and $v_{\mathrm{pv}}(K)$ are the current and voltage of the PV panel measured at a given operating point in step K. The g_{ac} is estimated as

$$\hat{g}_{\mathrm{ac}} = -\frac{i_{\mathrm{pv}}(K) - i_{\mathrm{pv}}(K-1)}{v_{\mathrm{pv}}(K) - v_{\mathrm{pv}}(K-1)}. \tag{6}$$

With these, the new operating point is given by

$$d(K+1) = \begin{cases} d(K) + \Delta d & \text{if } \hat{\mathrm{G}}_{\mathrm{dc}}(K) > \hat{\mathrm{g}}_{\mathrm{ac}}(K) \\ d(K) - \Delta d & \text{if } \hat{\mathrm{G}}_{\mathrm{dc}}(K) < \hat{\mathrm{g}}_{\mathrm{ac}}(K) \end{cases} \tag{7}$$

where $d(K)$ is the converter duty-cycle and Δd is the step-size of the algorithm. The selection of Δd and the time between MPP decisions (T_{MPPT}) has to selected based on the application and is one of the disadvantages of the InCond algorithm.

This algorithm has several disadvantages: 1) the continuous injection of a perturbation causes an oscillation in between three states that reduces the overall efficiency of the converter; 2) the fixed Δd and T_{MPPT} create a trade-off between accuracy (given by a smaller Δd) and speed (given by a larger Δd) and a balance has to be selected; 3) since the converter has to reach steady state to obtain a valid measurement, the T_{MPPT} is limited by the converter speed further compromising the tracking; 4) since changes in irradiance can happen in between samples errors can happen in the estimation of g_{ac} causing deviations in the operating conditions; and 5) the tracking of gradual changes in the irradiance is not accurate except when Δd coincides with the optimal changing rate [32]. The proposed LIA-based MPPT algorithm tackles those limitations.

III. Proposed LIA-Based MPPT

The InCond algorithm is based on the estimation of G_{dc} and g_{ac} by the difference between adjacent operating points; however, a more accurate estimation is proposed in this work. The proposed LIA-based MPPT algorithm is based on two fundamental elements: the use of the ripple injected by the power converter to estimate the g_{ac} and G_{dc} and the use of a digital Integral controller to regulate the difference to zero. The use of a power converter to adapt the voltage/current characteristics of the PV panel to the load and do the MPPT process introduces an inherent ripple to the PV panel controlled by f_{sw}, d and the reactive components of the topology (C and L). Using this ripple to estimate g_{ac} is particularly useful since: 1) it is already in the system, so no additional perturbation is injected; 2) it is small compared with the standard step-size of the InCond algorithm; 3) it is very fast, which allows for accurate tracking of changing conditions; and 4) it is more accurate since it measures the impedance around the operating point (tangent line) instead of between two adjacent points (secant line).

Two elements need to be identified for v_{pv} and i_{pv}: the average value (to calculate G_{dc}) and the fundamental components amplitude (to calculate g_{ac}). This is archived by sampling the ripple and applying some digital filters. The average value is extracted using the Moving Average Filter while the amplitude of ac component is extracted using the LIA. A block diagram of the extraction of this quantities in the system is presented in Fig. 4. More detail on this implementations is presented in Sections III-A and III-B.

Once G_{dc} and g_{ac} have been measured, the MPPT algorithm is targeted with keeping the difference between them zero. While traditional InCond implementations will check the difference and move the operating point one step in that direction, a simpler implementation can be made using an integral controller. Details of this implementation will be given in Section III-C.

A. Moving Average Filter

The MAF is a digital filter specially suited to extract the average value of a signal when it is contaminated with ac

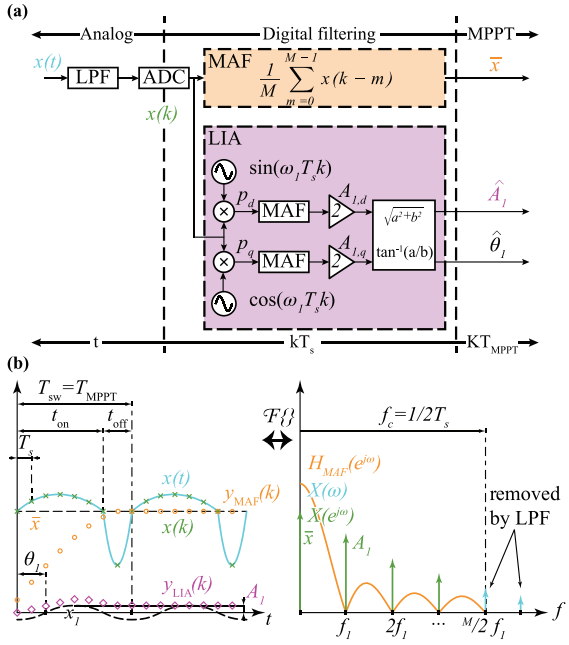

Fig. 4. (a) Block diagram of the MAF and the LIA are presented, preceded by the anti-aliasing filter and the ADC stage. (b) Time and frequency domain representation of the LIA, MAF, and input signals.

components of known harmonic frequency. Let $x(t)$ be a continuous-time signal like the one illustrated in Fig. 4(b)

$$x(t) = n(t) + \sum_{m=1}^{\infty} A_m \sin(\omega_1 m t + \theta_m) \tag{8}$$

where $n(t)$ is a band-limited signal, and A_m and θ_m are the amplitude and phase of the harmonic components at frequencies of $m\omega_1$. After an anti-aliasing filter and the sampling of the signal with a period T_s, $x(t)$ in the discrete domain is given by

$$x(k) = n(k) + \sum_{m=1}^{N_h} A_m \sin(\omega_1 m T_s k + \theta_m) \tag{9}$$

where N_h is the last harmonic allowed through the anti-aliasing filter. The spectrum of this signals is presented in Fig. 4(b) in the frequency domain. The MAF filter output $y(k)$ is given by

$$y(k) = \frac{1}{M} \sum_{m=0}^{M-1} x(k-m) \tag{10}$$

where M is the order of the filter and determines the frequencies that will be filtered. A more efficient implementation can be made using the infinite impulse response (IIR) version of the filter

$$y(k) = y(k-1) + \frac{x(k) - x(k-M)}{M}. \tag{11}$$

This version is extremely efficient to compute in real-time making the filter suitable for power electronics applications. The frequency response of the filter is given by

$$H_{\mathrm{MAF}}(e^{j\omega}) = \frac{1}{M} \frac{1 - e^{-j\omega M T_s}}{1 - e^{-j\omega T_s}}. \tag{12}$$

If T_s is selected such that

$$T_s = \frac{2\pi}{M\omega_1} \tag{13}$$

that is, the sampling frequency $(1/T_s)$ being exactly M times the fundamental frequency (f_1), the transfer function at ω_1 and all the harmonic frequencies $m\omega_1$ will be zero

$$H_{\mathrm{MAF}}(e^{j\omega_1 m}) = 0 \text{ for } m = 1, \ldots, M-1. \tag{14}$$

Leaving only the low-frequency spectrum $n(k)$. The output of the filter using the frequency response is

$$y(k) = H_{\mathrm{MAF}}(e^{j\omega}) * n(k) + \sum_{m=0}^{M-1} |H_{\mathrm{MAF}}(e^{j\omega_1 m})| A_m \sin(\omega_1 m T_s k + \theta_m - \theta_h) \tag{15}$$

that leads to

$$y(k) = H_{\mathrm{MAF}}(j\omega) * n(k) \tag{16}$$

which gives approximately the average value of the signal x

$$y(k) \approx \bar{n}(k) = \bar{x}(k). \tag{17}$$

The output of the MAF can be seen in Fig. 4(b) in yellow. The filter extracts the average value eliminating the ac components.

In order to make use of the switching ripple for the application, ω_1 is set to $2\pi f_{\mathrm{sw}}$, making the filter able to remove any trace of the switching oscillation from v_{pv} and i_{pv} every cycle of the PWM and to calculate G_{dc}. It will also be used as part of the LIA.

B. Lock-In Amplifier

To extract the amplitude of the fundamental component a LIA is used. As indicated in Fig. 4, the signal $x(k)$ is multiplied by a sine and cosine functions to produce the direct and quadrature components as

$$\begin{aligned} p_d(k) &= x(k)\sin(\omega_1 T_s k) \\ &= n(k)\sin(\omega_1 T_s k) \\ &\quad + \sum_{m=1}^{N_h} \frac{A_m}{2} \left(\cos(\omega_1 (m-1) T_s k + \theta_m) \right. \\ &\quad \left. - \cos(\omega_1 (m+1) T_s k + \theta_m)\right) \end{aligned} \tag{18}$$

$$\begin{aligned} p_q(k) &= x(k)\cos(\omega_1 T_s k) \\ &= n(k)\cos(\omega_1 T_s k) \\ &\quad + \sum_{m=1}^{N_h} \frac{A_m}{2} \left(\sin(\omega_1 (m-1) T_s k + \theta_m) \right. \\ &\quad \left. + \sin(\omega_1 (m+1) T_s k + \theta_m)\right). \end{aligned} \tag{19}$$

This has the effect of demodulating the fundamental component and move it to the base band while simultaneously moving the other components up in frequency, including the low-frequency

part $n(k)$. After that, two MAF are implemented to extract the average values

$$\bar{p}_{d,\mathrm{MAF}} \approx \frac{A_1}{2}\cos(\theta_1) \tag{20}$$

$$\bar{p}_{q,\mathrm{MAF}} \approx \frac{A_1}{2}\sin(\theta_1) \tag{21}$$

and the amplitudes are calculated as

$$A_{1,d} = 2\bar{p}_{d,\mathrm{MAF}} \tag{22}$$

$$A_{1,q} = 2\bar{p}_{q,\mathrm{MAF}}. \tag{23}$$

With $A_{1,d}$ and $A_{1,q}$, the total amplitude is calculated

$$\hat{A}_1 = \sqrt{A_{1,d}^2 + A_{1,q}^2} \tag{24}$$

the phase shift is

$$\hat{\theta}_1 = \tan^{-1}\left(\frac{A_{1,q}}{A_{1,d}}\right). \tag{25}$$

The output of the LIA can be seen in Fig. 4(b) in purple. The filter extracts amplitude of the first harmonic as a constant value. The use of this filter allows to accurately extract the average value of the first harmonic of the ripple in v_{pv} and i_{pv} every cycle of the PWM and to calculate g_{ac}. Given the small amplitude of both ripples around the dc operating point in the PV application, the system can be considered linear around each operating point and, therefore, amplitude of each individual harmonic can be used to measure g_{ac} at that frequency.

C. MPP Regulator

Once G_{dc} and g_{ac} have been determined, the objective of the MPPT algorithm is to make them equal

$$G_{\mathrm{dc}} - g_{\mathrm{ac}} = 0. \tag{26}$$

While the traditional InCond would compare the two values and step in one direction based on the difference and the previous step, a simpler solution can be implemented. By selecting the step-size to be proportional to the difference between the two resistances, we get

$$d(K+1) = d(K) + K_I(G_{\mathrm{dc}} - g_{\mathrm{ac}}) \tag{27}$$

where $d(K)$ is the duty-cycle in step K and K_I is the proportionality constant, we get a behavior that is very well known: it corresponds to a digital Integral Controller ($I(z)$) that regulates the difference between the two conductance to be zero. It is important to note that K indicates the step for the MPPT while k indicates the step for the filters. The MPPT happens at switching speed ($1/f_s$) while the digital filters use a faster sampling rate given by the MAF order M.

In summary, the proposed LIA-based MPPT algorithm uses an MAF and LIA to accurately measure G_{dc} and g_{ac} and a simple $I(z)$ achieving zero steady-state error and adaptive-step characteristics. The implementation of the filters is computationally efficient and the tuning of K_I is simple given its well known behavior.

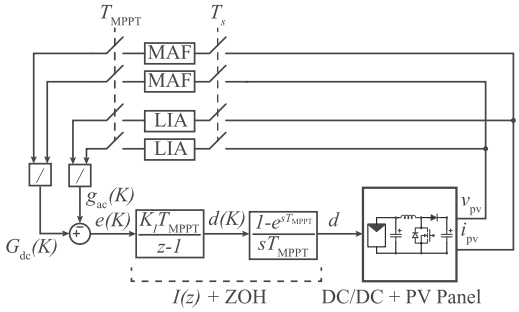

Fig. 5. Block diagram of the LIA-based MPPT algorithm with the control loop to evaluate stability.

D. Stability of the Proposed MPPT

In order to evaluate the stability of the proposed LIA-based MPPT strategy, a small signal model of the plant and controller around the MPP is developed. A block diagram of the system is presented in Fig. 5, where G_{dc} is obtained by the MAF and g_{ac} is obtained with LIA. The digital controller is evaluated once every MPPT sample period (T_{MPPT}) indicated by the index K. The new duty cycle $d(K)$ is determined by the integral controller $I(z)$ to produce the adaptive-step and passed through the zero-order-hold to the continuous time domain. The dc/dc converter and PV panel are modeled by H_{dv}. It is important to note that the sample time of the MAF and LIA T_s is M-times smaller and indicated by the index k; the output of the filters is evaluated only once per MPPT cycle resulting in a cycle average and avoiding the interaction between the filters and the control loop.

The small signal averaged transfer function of the converter around the MPP is given by

$$H_{\mathrm{dv}}(s) = \frac{-V_{\mathrm{link}}}{L_b C_b s^2 + L_b G_{\mathrm{MPP}} s + 1}. \tag{28}$$

The error signal e is given by the MPP criteria given in (4) and it can be re written as

$$e = \frac{i_{\mathrm{pv}}}{v_{\mathrm{pv}}} - \frac{\mathrm{d}i_{\mathrm{pv}}}{\mathrm{d}v_{\mathrm{pv}}}. \tag{29}$$

A linearization of e around the MPP is given by

$$\begin{aligned} e(v_{\mathrm{pv}}, i_{\mathrm{pv}}) \approx\, & e(V_{\mathrm{MPP}}, I_{\mathrm{MPP}}) \\ & + \left.\frac{\partial e(v_{\mathrm{pv}}, i_{\mathrm{pv}})}{\partial v_{\mathrm{pv}}}\right|_{V_{\mathrm{MPP}}, I_{\mathrm{MPP}}} (v_{\mathrm{pv}} - V_{\mathrm{MPP}}) \\ & + \left.\frac{\partial e(v_{\mathrm{pv}}, i_{\mathrm{pv}})}{\partial i_{\mathrm{pv}}}\right|_{V_{\mathrm{MPP}}, I_{\mathrm{MPP}}} (i_{\mathrm{pv}} - I_{\mathrm{MPP}}). \end{aligned} \tag{30}$$

Considering the approximation of i_{pv} around the MPP given by

$$i_{\mathrm{pv}} \approx 2I_{\mathrm{MPP}} - G_{\mathrm{MPP}} v_{\mathrm{pv}} \tag{31}$$

the e signal can be estimated as

$$e(v_{\mathrm{pv}}, i_{\mathrm{pv}}) \approx 2G_{\mathrm{MPP}} - 2\frac{G_{\mathrm{MPP}}}{V_{\mathrm{MPP}}} v_{\mathrm{pv}}. \tag{32}$$

The small-signal, averaged e is given by

$$\hat{e}(v_{\mathrm{pv}}, i_{\mathrm{pv}}) \approx -2\frac{G_{\mathrm{MPP}}}{V_{\mathrm{MPP}}} \hat{v}_{\mathrm{pv}}. \tag{33}$$

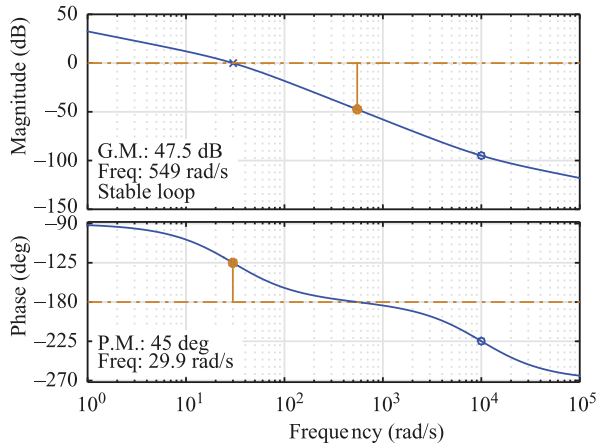

Fig. 6. Frequency response of the system with the proposed LIA-based MPPT indicating gain margin (GM) and phase margin (PM) for stability.

The change in the duty-cycle is given by

$$\hat{d}(z) = \left(-2\frac{G_{\mathrm{MPP}}}{V_{\mathrm{MPP}}}\hat{v}_{\mathrm{pv}}\right)\frac{K_I T_{\mathrm{MPPT}}}{z-1} \tag{34}$$

and after the ZOH, the continuous time duty-cycle is given by

$$\frac{\hat{d}(s)}{\hat{v}_{\mathrm{pv}}(s)} = -2\frac{G_{\mathrm{MPP}}}{V_{\mathrm{MPP}}}\frac{K_I T_{\mathrm{MPPT}}}{e^{sT_{\mathrm{MPPT}}}-1}\frac{1-e^{-sT_{\mathrm{MPPT}}}}{sT_{\mathrm{MPPT}}}. \tag{35}$$

The time delay $e^{sT_{\mathrm{MPPT}}}$ can be approximated by Taylor's expansion as $(1 - sT_{\mathrm{MPPT}})$. This model yields the following expression for the voltage-to-duty-cycle transfer function

$$\frac{\hat{d}(s)}{\hat{v}_{\mathrm{pv}}(s)} = -2\frac{G_{\mathrm{MPP}}}{V_{\mathrm{MPP}}}\frac{K_I(1-sT_{\mathrm{MPPT}})}{s}. \tag{36}$$

The characteristic equation is given by

$$H(s) = 1 + 2\frac{K_I G_{\mathrm{MPP}} V_{\mathrm{link}}}{V_{\mathrm{MPP}}}\frac{(1-sT_{\mathrm{MPPT}})}{L_b C_b s^3 + L_b G_{\mathrm{MPP}} s^2 + s}. \tag{37}$$

The range of stable values for K_I will depend on the system parameters as well as T_{MPPT} as expected. The bode plot for the system parameters simulated is presented in Fig. 6, it shows the gain and phase margins available for the system. With this model the range stable values for K_I in each application can be determined.

IV. Simulation Results

The results of the computer simulation for both the LIA-based MPPT and the standard InCond for a start-up transient and a series of changes in irradiance are presented in this section. The model consists of a PV panel connected to a constant dc bus through a boost converter and the MPPT controller to determine the duty cycle of the converter. The analog stages and quantization of ADC are implemented in the model to better reflect the behavior of the platform. The results of the simulations are presented in the normalized domain, where the normalization factors are the MPP I^o_{MPP}, V^o_{MPP}, and P^o_{MPP} in standard test conditions (1 Sun, 25°C). The f_{sw} is set to 10 kHz and f_s to 80 kHz which makes the order of the MAF 8. The

TABLE I
Simulation Transients Implemented to Test MPPT Algorithms

Label	Initial G [Sun]	Final G [Sun]	Speed [Sun/s]
Ⓐ	0.6	1.0	40
Ⓑ	1.0	0.3	−70
Ⓒ	0.3	1.0	7
Ⓓ	1.0	0.3	−7

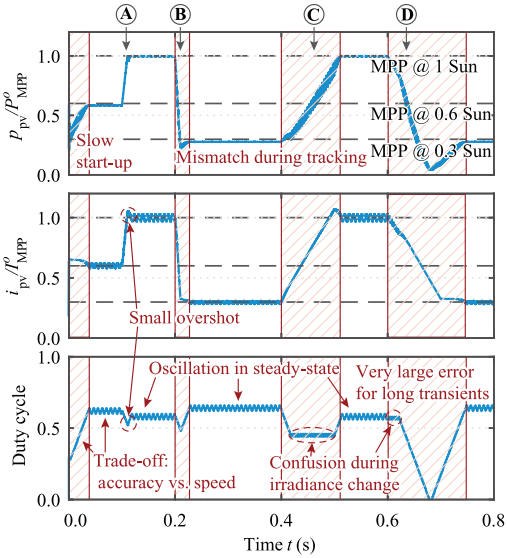

Fig. 7. Simulations of the standard InCond for a start-up transient followed by the four transients Ⓐ, Ⓑ, Ⓒ, and Ⓓ; details of these transients will be presented in the following figures.

details of the transients implemented are presented in Table I, each transient is assigned a label (Ⓐ, Ⓑ, Ⓒ, and Ⓓ) to track them through the different simulation captures and domains.

The simulation results for the standard InCond algorithm are presented in Fig. 7 while the results for the proposed LIA-based MPPT are presented in Fig. 8. The standard InCond presents a slower start-up time and oscillations in steady state; the tracking speed and accuracy are balanced by the step-size and constitute a tradeoff between the factors. During the transients (Ⓐ, Ⓑ, Ⓒ, and Ⓓ), confusions can happen based on the direction of the irradiance change and the previous step-direction. Even when tracking in the correct direction, the InCond algorithm is prone to overshoot if the tracking speed does not exactly match the irradiance change speed. These oscillations, delays, errors and overshoots contribute to reducing the tracking efficiency of the algorithm.

The proposed LIA-based MPPT algorithm solves all those issues effectively. Using the LIA and the inherent switching ripple of the converter, it is possible to produce smooth operation in steady state when changes are not required maximizing the extracted power ❶, the adaptive-step feature allows the quick and accurate start-up of the system ❷, and the combination of both allows to clearly identify the changes in irradiance and track them ❸. From Fig. 8, the benefits of the proposed LIA-based MPPT are evident.

A comparison of the transient tracking capabilities of both algorithms is presented in Fig. 9 for the transients Ⓐ, Ⓑ, Ⓒ, and Ⓓ in Figs. 7 and 8. The proposed LIA-based MPPT keeps

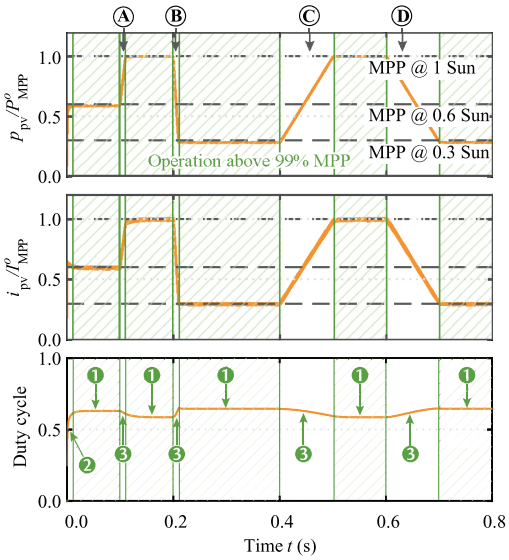

Fig. 8. Simulations of the LIA-based MPPT for a start-up followed by the four transients Ⓐ, Ⓑ, Ⓒ, and Ⓓ; the key benefits ❶, ❷, and ❸ are indicated.

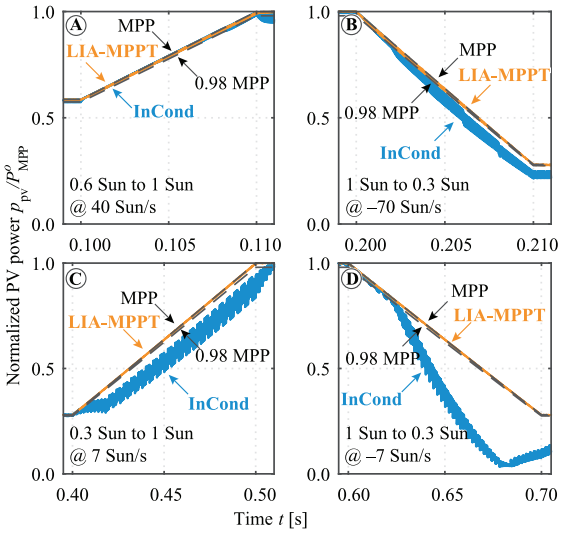

Fig. 9. Detail of the transients Ⓐ, Ⓑ, Ⓒ, and Ⓓ simulated compared with the ideal MPP and the 98% mark.

the tracking within 98% of the MPP during all the transients, while the standard InCond deviates notably during the transient.

The same transients can be observed in Fig. 10 in the phase plane (V/I). Again, it can be observed how the proposed MPPT has a superior performance operating over the optimal line while the standard InCond algorithm deviates visibly from that optimal trajectory. The labels Ⓐ, Ⓑ, Ⓒ, and Ⓓ indicate the trajectory of the InCond algorithm, since the LIA-based MPPT stays very close to the optimal line. Transient Ⓓ shows a very large drop for the InCond, this is caused by the typical confusion of the standard InCond algorithm due to the overall power decreasing for a long time; the proposed LIA-based algorithm does not present this problem, producing accurate tracking all the time.

The selection of K_I influences the transient effects in the same way as any control loop. The effects of this parameter for

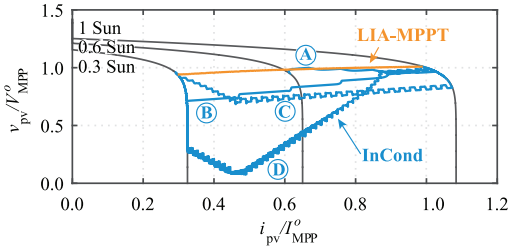

Fig. 10. $V-I$ plane representation of the transients Ⓐ, Ⓑ, Ⓒ, and Ⓓ for the proposed LIA-based MPPT and the standard InCond algorithms.

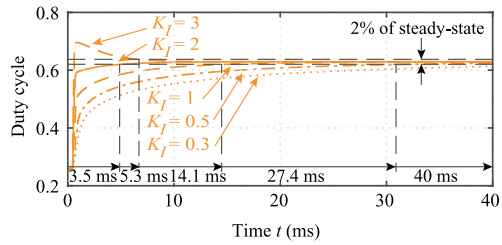

Fig. 11. Influence of the selection of the integral gain K_I on the tracking capabilities of the LIA-based MPPT.

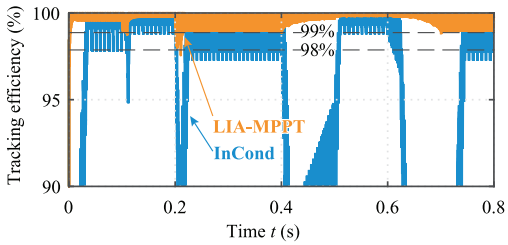

Fig. 12. Tracking efficiency of the LIA-based MPPT and the standard InCond during the simulation.

a range of $0.3-3$ are shown in Fig. 11. Even when the whole range of parameters produces stable behavior, the selection can lead to faster tracking or have overshoot when it is not properly selected. For this simulations, the value of 2 was selected for K_I.

Finally, a summary of the tracking efficiency of both algorithms during the complete simulation can be observed in Fig. 12. The curves show how the proposed MPPT keeps the efficiency within 98% all the time and within 99% in steady state. The variations in the efficiency have one component for the proposed LIA-based MPPT (the switching ripple) and an additional component for the InCond MPPT (the oscillation in steady state). The efficiency is lower at lower irradiance since the step-size is constant and v_{MPP} is not linearly dependent on the irradiance, leading to a proportionally larger loss due to the variation at lower irradiance. This is coherent with the logarithmic dependency of v_{MPP} with the irradiance. The standard InCond produces much lower efficiency specially during the transients where it goes below the top 10%.

V. Experimental Results

In order to validate the proposed MPPT algorithm and compare against the standard InCond algorithm, an experimental test was developed as can be seen in Fig. 13; the summary of

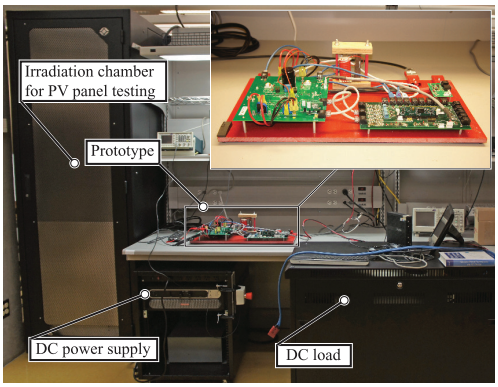

Fig. 13. Experimental setup with a zoom-in of the prototype.

TABLE II
EXPERIMENTAL SET-UP PARAMETERS

Parameter	Value
C_b	470 nF
L_b	2.2 mH
f_{sw}	10 kHz
f_s	80 kHz
f_c	40 kHz
M	8
$T_{\mathrm{MPPT},InC}$	2 ms
Δd_{fast}	2%
Δd_{slow}	1%
Voltage range	0 to 30 V
Current range	0 to 6 A

the system parameters are presented in Table II. Two step-sizes are considered for the InCond during the experiments in order to compare a precise but slow version and a fast but inaccurate version. A boost converter was implemented controlled by an industry-standard microcontroller (C2000) typically employed to control power converters.

The experimental results for the steady-state operation of the prototype are presented in Fig. 14. The standard resolution shows no oscillation in steady state and a smooth behavior, a desirable operating mode to maximize the energy extracted, with no three state oscillation that reduces the efficiency. The zoom-in section to the right shows the switching oscillation that is isolated by the LIA to extract the InCond. This small ripple is characteristic of the system, as opposed to the injected by the InCond algorithm to locate the MPP. The LIA is able to extract the small value ignoring the noise, while the computation time for this configuration was measured in less than 1.6 µs per sample, which would allow to push the switching frequency further up if required.

Experimental results for transients are presented in Fig. 15 for the proposed LIA-based MPPT and in Figs. 16 and 17 for the traditional InCond with two different steps-sizes (fast and slow). The irradiation of the PV panel is changed during the transient, the speed of change is limited by the lamps used to generate the profile. It can be observed how the proposed LIA-based MPPT is able to track the MPP in a smooth way as observed in the simulations. The InCond with a small tracking step produces smaller oscillations in steady state, but is not able

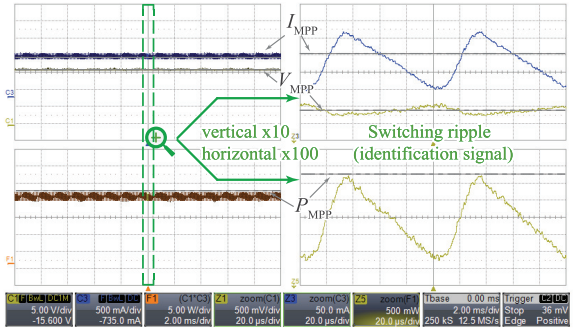

Fig. 14. Steady-state experimental capture of the proposed LIA-based MPPT; the zoom shows the small switching ripple used to identify g_{ac}.

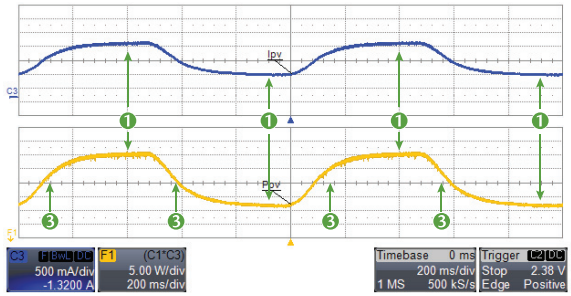

Fig. 15. Transient experimental capture of the proposed LIA-based MPPT; it benefits from the ❶ eliminated oscillation, the small-signal identification, and ❸ adaptive-step.

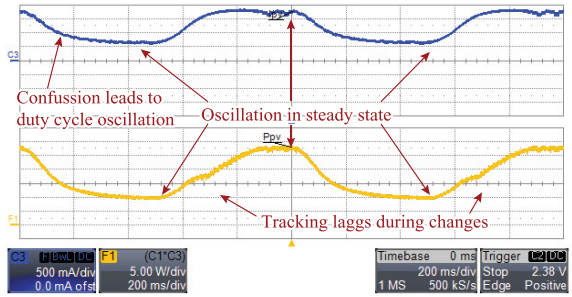

Fig. 16. Transient experimental capture of the traditional InCond algorithm with a small tracking-step.

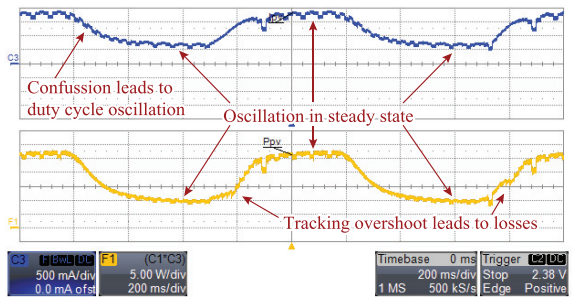

Fig. 17. Transient experimental capture of the traditional InCond algorithm with a large tracking-step.

to track the MPP during changing conditions, producing a lagging result. The InCond with a large step-size can track faster but has occasional overshoots and a much larger oscillation in steady state which lead to a loss in efficiency. Proper tuning

TABLE III
COMPARISON OF THE PROPOSED LIA-BASED MPPT ALGORITHM WITH THE STANDARD INCOND AND FOUR ADVANCED MPPT ALGORITHMS

Algorithm	Loops	Perturbation	τ_o[a]	Notes
InCond (Δd_{fast})	MPPT	Fixed	742	Baseline comparison algorithm
LIA-based	MPPT	None	20	Tracking of transient slopes and steps are optimized; computational cost is higher
Sliding mode	V + MPPT	Fixed	405	Control is based on Sliding mode, while MPPT is based on InCond; Tracking of slope changes shows problems as InCond
Locus-based	I + MPPT	Fixed[b]	187	Requires off-site characterization
Emulated resistance	V + MPPT	V_{oc} measured	74	Requires off-site characterization and temperature characterization; requires periodic measurement of V_{oc}
Variable-step (β)	MPPT	Variable[c]	52	Requires off-site characterization and temperature characterization and irradiance tuning for β

[a]Tracking time normalized to the converter resonance frequency $\tau_o = T_o/(2\pi\sqrt{\mathrm{LC}})$.
[b]Fixed step is used in steady state, the large tracking is done in steady state, the large tracking is done with the locus-based method with the locus-based method.
[c]Reduced until a minimum value.

leads to a balance for a given slope, panel, and oscillation but the benefits are lost if the irradiance change slope is modified.

The comparison of the proposed LIA-based MPPT algorithm was performed against the standard InCond. This provides a reference point to compare with advanced MPPT algorithms. A comparison of the proposed LIA-based MPPT with other advanced MPPT algorithms was performed in Table III; the selected algorithms are presented for their advanced features that allow for fast tracking and account for environmental changes. Since the tracking speed is highly dependent on the size of the converter, the tracking time is normalized with respect to the resonance frequency of the converter (for those documents that provide said values). The selected algorithms use InCond versions with adaptive-step (such as the β algorithm or very high-speed controllers such as the sliding mode controller to increase the speed. The proposed algorithm benefits from the single loop MPPT-oriented control to increase the speed and the LIA and MAF to reduce the perturbation size allowing fast, accurate and smooth behavior.

Although the proposed technique presents higher computational demand for the sampling and filters compared with standard MPPT algorithms, the accuracy of the removal of the perturbation that leads to higher steady-state efficiency, the ability to identify the changes and adaptive the step-size obtained are a significant advantage over more simple algorithms. Normal digitally-controlled power converters sample several times per switching cycle in order to average the behavior of the current/voltage, and the processing power of industry standard microcontroller (C2000) is capable of handling this load. The benefits of the proposed implementation, with smooth operation and adaptive tracking speed become evident when compared with the standard MPPT algorithms.

VI. CONCLUSION

A new LIA-based MPPT algorithm for PV panels was presented in this paper. This algorithm used the inherent ripple in power electronics converters combined with the moving average filter and the LIA to produce accurate tracking of the MPP even in the presence of changes in the environmental conditions without the need of injecting any kind of disturbance to the system or include any aditional sensors. An Integral controller was used to produce an adaptive-step feature for variable tracking speed that allows for fast tracking and its stability was studied based on the small signal model. The combination of these characteristics produced: 1) smooth operation in steady-steady state maximizing the transferred power and removing the characteristic oscillations of standard MPPT algorithms; 2) fast and accurate tracking during start-up; and 3) irradiance change identification and tracking for variable change rates. The proposed algorithm was studied with simulations and validated with experimental results implemented in an industry-standard microcontroller. A comparison of the results of the proposed MPPT algorithm is performed against several modern MPPT algorithms to highlight the benefits and drawbacks. The performance improvements provided by the proposed algorithm both in steady state and during transients show the benefits of using the inherent ripple as identification signal and the simple integral controller for adaptive-step.

REFERENCES

[1] M. de Brito, L. Galotto, L. Sampaio, G. de Azevedo e Melo, and C. Canesin, "Evaluation of the main MPPT techniques for photovoltaic applications," *IEEE Trans. Ind. Electron.*, vol. 60, no. 3, pp. 1156–1167, Mar. 2013.
[2] B. Subudhi and R. Pradhan, "A comparative study on maximum power point tracking techniques for photovoltaic power systems," *IEEE Trans. Sustain. Energy*, vol. 4, no. 1, pp. 89–98, Jan. 2013.
[3] T. Esram and P. Chapman, "Comparison of photovoltaic array maximum power point tracking techniques," *IEEE Trans. Energy Convers.*, vol. 22, no. 2, pp. 439–449, Jun. 2007.
[4] S. Kjaer, "Evaluation of the "hill climbing" and the "incremental conductance" maximum power point trackers for photovoltaic power systems," *IEEE Trans. Energy Convers.*, vol. 27, no. 4, pp. 922–929, Dec. 2012.
[5] K. Ishaque and Z. Salam, "A deterministic particle swarm optimization maximum power point tracker for photovoltaic system under partial shading condition," *IEEE Trans. Ind. Electron.*, vol. 60, no. 8, pp. 3195–3206, Aug. 2013.
[6] H. Renaudineau *et al.*, "A PSO-based global MPPT technique for distributed PV power generation," *IEEE Trans. Ind. Electron.*, vol. 62, no. 2, pp. 1047–1058, Feb. 2015.
[7] A. Chikh and A. Chandra, "An optimal maximum power point tracking algorithm for PV systems with climatic parameters estimation," *IEEE Trans. Sustain. Energy*, vol. 6, no. 2, pp. 644–652, Apr. 2015.
[8] M. Sheraz and M. Abido, "An efficient approach for parameter estimation of PV model using de and fuzzy based MPPT controller," in *Proc. IEEE Conf. Evolv. Adapt. Intell. Syst. (EAIS)*, Jun. 2014, pp. 1–5.
[9] C. Sullivan, J. Awerbuch, and A. Latham, "Decrease in photovoltaic power output from ripple: Simple general calculation and the effect of partial shading," *IEEE Trans. Power Electron*, vol. 28, no. 2, pp. 740–747, Feb. 2013.

[10] R. Faranda, S. Leva, and V. Maugeri, 'MPPT techniques for PV systems: Energetic, and cost comparison," in *Proc. IEEE Power Energy Soc. Gen. Meeting Convers. Del. Elect. Energy 21st Century*, Pittsburgh, PA, USA, Jul. 2008, pp. 1–6.
[11] Y. Levron and D. Shmilovitz, "Maximum power point tracking employing sliding mode control," *IEEE Trans. Circuits Syst. I, Reg. Papers*, vol. 60, no. 3, pp. 724–732, Mar. 2013.
[12] M. Sokolov and D. Shmilovitz, "A modified MPPT scheme for accelerated convergence," *IEEE Trans. Energy Convers.*, vol. 23, no. 4, pp. 1105–1107, May 2008.
[13] S. Jain and V. Agarwal, "A new algorithm for rapid tracking of approximate maximum power point in photovoltaic systems," *Power Electron. Lett.*, vol. 2, no. 1, pp. 16–19, 2004.
[14] N. Femia, G. Petrone, G. Spagnuolo, and M. Vitelli, "Optimization of perturb and observe maximum power point tracking method," *IEEE Trans. Power Electron.*, vol. 20, no. 4, pp. 963–973, Jul. 2005.
[15] A. Latham, R. Pilawa-Podgurski, K. Odame, and C. Sullivan, "Analysis and optimization of maximum power point tracking algorithms in the presence of noise," *IEEE Trans. Power Electron.*, vol. 28, no. 7, pp. 3479–3494, Jul. 2013.
[16] P. Manganiello, M. Ricco, G. Petrone, E. Monmasson, and G. Spagnuolo, "Optimization of perturbative PV MPPT methods through online system identification," *IEEE Trans. Ind. Electron.*, vol. 61, no. 12, pp. 6812–6821, Dec. 2014.
[17] M. Mohd Zainuri, M. Mohd Radzi, A. Soh, and N. Rahim, "Development of adaptive perturb and observe-fuzzy control maximum power point tracking for photovoltaic boost dc-dc converter," *IET Renew. Power Gener.*, vol. 8, no. 2, pp. 183–194, Mar. 2014.
[18] M. Killi and S. Samanta, "An adaptive voltage-sensor-based MPPT for photovoltaic systems with SEPIC converter including steady-state and drift analysis," *IEEE Trans. Ind. Electron.*, vol. 62, no. 12, pp. 7609–7619, Dec. 2015.
[19] P. Manganiello, M. Ricco, G. Petrone, E. Monmasson, and G. Spagnuolo, "Dual-Kalman-filter-based identification and real-time optimization of PV systems," *IEEE Trans. Ind. Electron.*, vol. 62, no. 11, pp. 7266–7275, Nov. 2015.
[20] M. Ricco, P. Manganiello, E. Monmasson, G. Petrone, and G. Spagnuolo, "FPGA-based implementation of dual Kalman filter for PV MPPT applications," *IEEE Trans. Ind. Informat.*, to be published, doi: 10.1109/TII.2015.2462313.
[21] M. Elgendy, B. Zahawi, and D. Atkinson, "Assessment of perturb and observe MPPT algorithm implementation techniques for PV pumping applications," *IEEE Trans. Sustain. Energy*, vol. 3, no. 1, pp. 21–33, Jan. 2012.
[22] M. Elgendy, B. Zahawi, and D. Atkinson, "Assessment of the incremental conductance maximum power point tracking algorithm," *IEEE Trans. Sustain. Energy*, vol. 4, no. 1, pp. 108–117, Jan. 2013.
[23] D. Sera, R. Teodorescu, J. Hantschel, and M. Knoll, "Optimized maximum power point tracker for fast-changing environmental conditions," *IEEE Trans. Ind. Electron.*, vol. 55, no. 7, pp. 2629–2637, Jul. 2008.
[24] H. Zhu, D. Zhang, H. Athab, B. Wu, and Y. Gu, "PV isolated three-port converter and energy-balancing control method for PV-battery power supply applications," *IEEE Trans. Ind. Electron.*, vol. 62, no. 6, pp. 3595–3606, Jun. 2015.
[25] M. Boztepe, F. Guinjoan, G. Velasco-Quesada, S. Silvestre, A. Chouder, and E. Karatepe, "Global MPPT scheme for photovoltaic string inverters based on restricted voltage window search algorithm," *IEEE Trans. Ind. Electron.*, vol. 61, no. 7, pp. 3302–3312, Jul. 2014.
[26] W. Chen and C. Tsai, "Optimal balancing control for tracking theoretical global MPP of series PV modules subject to partial shading," *IEEE Trans. Ind. Electron.*, vol. 62, no. 8, pp. 4837–4848, Aug. 2015.
[27] J. Ahmed and Z. Salam, "An improved method to predict the position of maximum power point during partial shading for PV arrays," *IEEE Trans. Ind. Informat.*, vol. 11, no. 6, pp. 1378–1387, Dec. 2015.
[28] S. Lyden and M. Haque, "A simulated annealing global maximum power point tracking approach for PV modules under partial shading conditions," *IEEE Trans. Power Electron.*, vol. 31, no. 6, pp. 4171–4181, Jun. 2016.
[29] Y. Wang, Y. Li, and X. Ruan, "High-accuracy and fast-speed MPPT methods for PV string under partially shaded conditions," *IEEE Trans. Ind. Electron.*, vol. 63, no. 1, pp. 235–245, Jan. 2016.
[30] Y. Shi, R. Li, Y. Xue, and H. Li, "High-frequency-link-based grid-tied PV system with small dc-link capacitor and low-frequency ripple-free maximum power point tracking," *IEEE Trans. Power Electron.*, vol. 31, no. 1, pp. 328–339, Jan. 2016.
[31] J. Galvez and M. Ordonez, "Swinging bus operation of inverters for fuel cell applications with small dc-link capacitance," *IEEE Trans. Power Electron.*, vol. 30, no. 2, pp. 1064–1075, Feb. 2015.
[32] F. Paz and M. Ordonez, "Zero oscillation and irradiance slope tracking for photovoltaic MPPT," *IEEE Trans. Ind. Electron.*, vol. 61, no. 11, pp. 6138–6147, Nov. 2014.
[33] F. Paz and M. Ordonez, "Fast and efficient solar incremental conductance MPPT using lock-in amplifier," in *Proc. 6th IEEE Int. Symp. Power Electron. Distrib. Gener. Syst. (PEDG)*, Aachen, Germany, Jun. 2015, pp. 363–368.
[34] A. Bazzi and P. Krein, "Ripple correlation control: An extremum seeking control perspective for real-time optimization," *IEEE Trans. Power Electron.*, vol. 29, no. 2, pp. 988–995, Feb. 2014.
[35] C. Barth and R. Pilawa-Podgurski, "Dithering digital ripple correlation control for photovoltaic maximum power point tracking," *IEEE Trans. Power Electron.*, vol. 30, no. 8, pp. 4548–4559, Aug. 2015.
[36] X. Lin, Y. Wang, M. Pedram, J. Kim, and N. Chang, "Event-driven and sensorless photovoltaic system reconfiguration for electric vehicles," in *Proc. Des. Autom. Test Eur. Conf. Exhib. (DATE)*, Mar. 2015, pp. 19–24.
[37] A. Marzouk, S. Fournier-Bidoz, J. Yablecki, K. McLean, and O. Trescases, "Analysis of partial power processing distributed MPPT for a PV powered electric aircraft," in *Proc. Int. Power Electron. Conf. (IPEC-Hiroshima ECCE-ASIA)*, May 2014, pp. 3496–3502.
[38] G. Tsekouras, F. Kanellos, and J. Prousalidis, "Simplified method for the assessment of ship electric power systems operation cost reduction from energy storage and renewable energy sources integration," *IET Elect. Syst. Transp.*, vol. 5, no. 2, pp. 61–69, Jun. 2015.
[39] M. Ordonez, M. Sonnaillon, J. Quaicoe, and M. Iqbal, "An embedded frequency response analyzer for fuel cell monitoring and characterization," *IEEE Trans. Ind. Electron.*, vol. 57, no. 6, pp. 1925–1934, Jun. 2010.
[40] R. Tanaka, M. Sasaki, and T. Shirane, "Temperature dependence of minor hysteresis loop in NiZn ferrite measured by lock-in amplifier," *IEEE Trans. Magn.*, vol. 51, no. 1, pp. 1–4, Jan. 2015.
[41] S. Arora, P. T. Balsara, D. K. Bhatia, R. J. Taylor, and B. Hunt, "Gain and Phase (Gap) measurement device," in *Proc. IEEE Appl. Power Electron. Conf. Expo. (APEC)*, Mar. 2015, pp. 2453–2458.

Francisco Paz (S'08) was born in La Plata, Argentina. He received the Ing. degree in electronics engineering from the National University of Comahue, Neuquen, Argentina, in 2012, and the M.A.Sc. degree in electrical engineering from The University of British Columbia (UBC), Vancouver, BC, Canada, in 2014. He is currently working toward the Ph.D. degree at UBC.

His research interests include renewable energy conversion, maximum power point tracking, and renewable energy system topologies for solar, wind, and marine power.

Mr. Paz was the recipient of several scholarships including one from the Argentinian Ministry of Education and the Ministry of Science, Technology, and Productive Innovation (2008), the ICICS Graduate Scholarship (2014), the Faculty of Applied Science Graduate Award (UBC, 2014 and 2015), and the Four Year Fellowship for Ph.D. students (2014) from UBC.

Martin Ordonez (S'02–M'09) was born in Neuquen, Argentina. He received the Ing. degree in electronics engineering from the National Technological University, Buenos Aires, Argentina, in 2003, and the M.Eng. and Ph.D. degrees from the Memorial University of Newfoundland (MUN), St. John's, NL, Canada, in 2006 and 2009, respectively.

He is a Canada Research Chair and an Associate Professor with The University of British Columbia (UBC), Vancouver, BC, Canada. He was also an Adjunct Professor with Simon Fraser University, Burnaby, BC, Canada, and MUN. His industrial experience includes R&D at Xantrex Technology Inc./Elgar Electronics Corp. (now AMETEK Programmable Power), Deep-Ing Electronica de Potencia, and TRV Dispositivos, Argentina. He became a Fellow of the School of Graduate Studies, MUN.

Dr. Ordonez is an Associate Editor of the IEEE TRANSACTIONS ON POWER ELECTRONICS, serves on several IEEE committees, and reviews widely for IEEE/IET. He was the recipient of the David Dunsiger Award for Excellence (2009) and the Chancellors Graduate Award/Birks Graduate Medal (2006).